



Next Generation Very Large Array Memo No. 114
June 12, 2023

High Dynamic Range Imaging at 8 GHz with Spiral and Core, including Phase Errors

C.L. Carilli

National Radio Astronomy Observatory, Socorro, NM, USA

Abstract

I investigate the ability of the ngVLA to make high dynamic range images of a complex, extended source with high and low surface brightness regions. The model is an altered version of the best Cygnus A image at 8 GHz from the VLA. This model includes spectral structure across the source in a spectral cube from 7 GHz to 9 GHz. The configuration includes all Spiral antennas (54) and 27 Core antennas. The simulations include thermal noise, plus two types of antenna-based phase errors: constant in time and frequency, and random in time and frequency. These two types bracket the possibilities. The results indicate that the ngVLA should be able to reach fidelity goals even for constant phase errors, and reach dynamic range requirements (depending on their definition), for random phase errors, but not constant phase errors.

1 Introduction

I investigate the ability of the ngVLA Spiral plus Core to make high fidelity, high dynamic range images of complex sources, including antenna-based phase errors. I also include a source model that has realistic spectral structure over a 25% bandwidth.

2 Model and Simulation

The source model is an adapted version of the VLA high dynamic range image of Cygnus A at 8 GHz. The image has a total flux density of 240 Jy, at an intrinsic resolution of $0.3''$. The total source extent is $120''$. The compact radio core, which gets convolved in the input model to $0.3''$, is blanked and replaced with a 1 Jy point source.

The intrinsic dynamic range of the input image is $\sim 10^4$. However, the image is then blanked at the 4σ level, with further by-hand blanking of higher residuals around the dominant hot spots at the end of the lobes, resulting in a model with no obvious extraneous structures. While the blanking process can be considered subjective, the fact remains that, whether using a doctored real-source model image, or a fabricated source of random geometric structures, the goal is simply to reproduce as closely as possible this input model, as judged by the resulting imaging artifacts and fidelity.

From a single frequency image, I generate a model spectral cube of 2 GHz total bandwidth with 21 spectral channels, centered at 8 GHz. The spectral channels are then scaled as a function of position and frequency by the VLA spectral index image of the source between 1.4 GHz and 5 GHz¹, to impose realistic spectral structure across the cube. In the faintest regions of the source, where the spectral index is not measured due to S/N limitations, a single value of -1.8 is used, consistent with the steepest measured spectral regions of the lobes.

CASA SIMOBSERVE was used to generate the visibility measurement sets. An 8 hour synthesis was employed with a record length of 120 seconds.

The configuration includes all 54 Spiral antennas, with a maximum baseline of 39 km, plus 27 Core antennas with projected baselines ranging from 4 km down to 50 m. The shortest baseline has a fringe spacing of $\sim 150''$ at 8 GHz. The UV-coverage for the 8 hr synthesis, including bandwidth synthesis, is shown in Figure 1.

Thermal noise is added to the visibilities. Antenna-based phase errors are then included in two ways. The first method assumes a constant phase error with time and frequency for each antenna, with a flat distribution in phase error per antenna over a range $= \pm 1^\circ$. The second includes the same flat error distribution range, but has random phase errors for each time record (120 s) and frequency channel (95 MHz). Note that a flat distribution in phase error over $\pm 1^\circ$ is very roughly comparable to a Gaussian distribution

¹The lower frequencies were used for spectral index to cover more of the faint radio lobes. A linear approximation to a powerlaw spectrum was employed over the ± 0.125 fractional bandwidth.

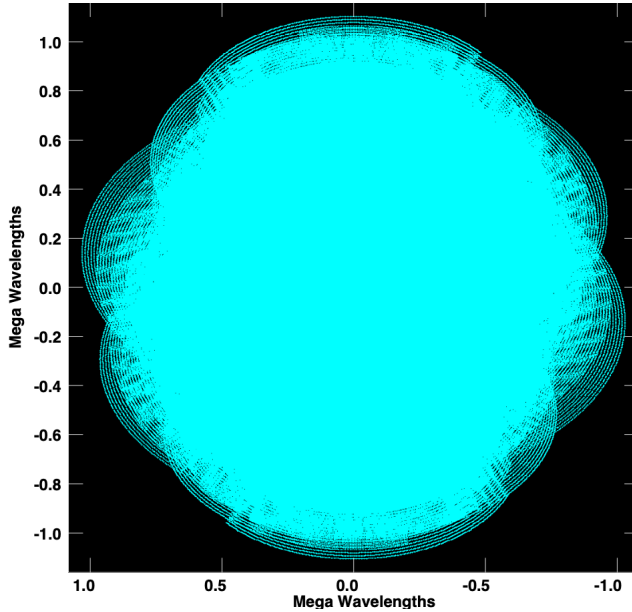


Figure 1: The UV coverage for the 8 hour synthesis including bandwidth synthesis from 7 GHz to 9 GHz, for the adopted configuration.

with an rms of $\sigma = 0.42^\circ$ (FWHM = 1°).

For the ngVLA project, the target rms phase errors at 8 GHz after calibration are $\sigma \sim 0.8^\circ$ (TK priv. comm.). The rms of the adopted errors is lower, implying good conditions, and/or with self-calibration. Note that the equations for the expected dynamic range due to phase errors for an interferometer are typically linear in phase rms and in the number of antennas (Perley 1998 SIRA II Chap 13; see below), so the results herein can be scaled linearly to larger or smaller values of σ .

Images were generated with TCLEAN using a multifrequency synthesis with $n_{\text{terms}} = 2$, plus multiscale clean (scales = 0,7,25), with Briggs weighting and a robust parameter of -0.5, using a CLEAN box around the source and 200000 iterations with a gain of 0.03. In all cases, TCLEAN cleans to a residual of 0.55 mJy, to a total cleaned flux density of 220 Jy.

2.1 Results

2.1.1 Dynamic Range

The resulting images are shown in Figure 2, including the input model convolved with the ngVLA PSF. The Gaussian fit to the PSF in CASA has a $\text{FWHM} = 0.20'' \times 0.17''$ at 81° . Shown are an image with just thermal noise, and one that also includes constant phase errors with time and frequency. The image with random phase errors looks very similar to the image with just thermal noise. The constant phase error images show more significant residuals in the vicinity of the bright hot spots (see below).

The images in Figure 2 have a peak surface brightness of $0.97 \text{ Jy beam}^{-1}$, corresponding to the point-source core. The total flux density in all three ngVLA simulated images is 224 Jy, slightly below the 240 Jy in the input model.

The peak surface brightness, besides the core, is the southern hot spot, with $0.60 \text{ Jy beam}^{-1}$. This region is generally the brightest and most complex in the source, so I calculate the image dynamic range by looking at the rms noise in the vicinity of the southern hot spot, but outside the radio source boundaries. The values of rms noise for the three images (thermal noise only, plus random phase errors, plus constant phase errors), are: 10, 13, and $48 \mu\text{Jy beam}^{-1}$, respectively. The implied dynamic range (hot spot peak/rms) are: 6.0×10^4 , 4.6×10^4 , and 1.2×10^4 , respectively. The maximum negative sidelobe around the southern hot spot in each case is: -0.15, -0.15, and $-0.37 \text{ mJy beam}^{-1}$.

In all cases the measured rms noise is well above the expected thermal naturally weighted noise of $0.31 \mu\text{Jy beam}^{-1}$ in 8 hours with 81 antennas, 2hrs, 2GHz bandwidth, ie. none of the images are thermal noise limited by a large factor, presumably due to limitations in the Fourier image restoration processes, such as gridding, deconvolution, and spectral model assumptions.

Considering the images with phase errors, approximations for the expected dynamic range for phase errors can be found in Perley (1998, SIRA II, equ. 13-8, 13-9). For antenna based phase errors constant in time and frequency, the expected value is: $\text{DNR} = N_{\text{ant}}/(\text{root}(2) \times \sigma)$, where N_{ant} is the number of antennas and σ is the rms of the phase errors in radians. For $\sigma \sim 0.42^\circ = 0.0072 \text{ rad}$, and 81 antennas, the expected $\text{DNR} = 8000$. This DNR is about 50% lower than the measured value in this image, which may have to do with the difference between the top hat phase error distribution used and a Gaussian distribution, or with the exact region chosen to make the measurement, or with the definition of dynamic range (see footnote).

For phase errors random in time and frequency, the predicted DNR increases by $\text{root}(N_{ind})$, where N_{ind} is the number of independent measurements $N_{ind} = N_{chans} \times N_{timerecords} = 21 \times 240$. This would increase the expected dynamic range due to the adopted phase errors to 6×10^5 , which is much larger than the measured value, meaning, the simulated image is limited by effects other than phase errors or thermal noise, as is also the case for just thermal noise. I note that the predicted dynamic ranges for phase errors are only approximations, and have been reconsidered in more detail recently (ngVLA memo 107). Moreover, the definition of dynamic range is ambiguous and not universal.²

One factor that has not been considered in the relationship between rms phase errors, N_{ant} , and image DNR, is weighting in the imaging stage. The equations in eg. Perley (1998), assume Natural weighting: effectively, every antenna gets the same weight. For robust weighting that approaches Uniform, the short spacing antennas may get significantly down weighted, meaning the 'effective N' decreases. One way of looking at this is that uniform weighting for an array with a dense Core like the ngVLA, is akin to simply using fewer Core antennas in the observation, meaning, lower N.

2.1.2 Fidelity

The image fidelity, defined as: $(\text{Model} - \text{Image})/\text{Model}$, where the Model has been convolved with the Gaussian CLEAN beam, is shown in Figure 3. Only regions with brightness $> 0.25 \text{ mJy beam}^{-1}$ are considered, corresponding to 5σ in the constant phase error image.

The image fidelity is high across the source, with a mean around zero and an rms of about 5% over the higher surface brightness regions, and 8% in the fainter tails of the radio lobes, including along the radio jet. There is a tendency for the fidelity to be systematically low in the fainter regions, meaning, model brighter than the image by $\sim 5\%$ on average. Such

²For reference, the target dynamic range requirement for deep fields at 8 GHz for the ngVLA is $\sim 3 \times 10^4$ (SCI 0113), but this definition is currently ill-defined since it uses: $DNR = (\text{quadrature sum of the brightest sources in the field}/rms)$, but it does not define how many sources should be used (see ngVLA memo 113). Hence, I consider the classic definition of $(DNR = \text{image peak surface brightness}/rms)$. This definition is consistent with Perley (1998 SIRA II chap 13). However, even this definition is incomplete: considering far sidelobes, the sidelobe-noise will be the RSS of the sidelobes from sources over the field; conversely, close to bright sources, the sidelobe noise will be dominated by the near sidelobes of the bright source itself. Generally, dynamic range may not be possible to define definitively, with different definitions appropriate for deep fields vs. complex, extended objects. Fidelity may be a clearer metric, in particular for extended sources.

a systematic offset might arise due to small differences between the true PSF and the assumed Gaussian used for convolution of the input model, for uncleaned residual emission. Note that the image fidelity was similar for all three simulated data sets, and hence only one example is shown. This similarity results from the fact that only higher brightness regions are considered in the analysis ($> 5\sigma$ in the highest noise image).

For reference, the target image fidelity requirement for the ngVLA is 10% (SCI 0108), which is well satisfied by the simulated observations, even with constant phase errors of the assumed magnitude.

2.1.3 Spectral Index

Figure 4 shows the resulting spectral index image from TCLEAN. Again, all three data sets produced a similar result, because only higher S/N regions are unblanked. Figure 4 also shows the spectral index ratio image = (model SI/image SI).

The resulting image spectral index distribution is qualitatively similar to the input model, with flat spectrum hot spots and steepening into the lobes. However, the SI ratio image shows that the resulting image spectral indices are systematically steeper than the input model (meaning, ratio values below 1). For the bright regions, this difference is between 10% and 20%. For the tails, this difference rises to a factor of two, meaning image spectral indices steeper than the input model by this factor. I do not know the origin of this difference between model and simulated spectral index images.

3 Conclusion

I explore image dynamic range and fidelity of Spiral plus some Core antennas for a complex source, including real spectral index structure in a multifrequency synthesis. The simulations included thermal noise, and phase errors that are constant in time and frequency, as well as those that are random in time and frequency, with an effective smoothing function in time and frequency of 120 s and 95 MHz, set by the record length and channel width. None of the resulting images reach the thermal noise by a large factor, meaning limitations are due to other process relating to Fourier image restoration.

All images have high fidelity, well within the ngVLA specification of 10%. The image with thermal noise only, and with random phase errors, both reach dynamic range specifications (at least within the definition adopted herein), that conform to ngVLA specifications, even scaled to the target

ngVLA phase rms specification of $\sigma = 0.8^\circ$. The constant phase error image does not reach ngVLA specifications in dynamic range. However, I consider such constant phase offsets in both time and frequency to be pessimistic and unlikely.

The resulting spectral index image has the correct qualitative spatial distribution, but the SI values are systematically steeper in the resulting image relative to the input model, by about 10% to 20% in bright regions, and up to a factor two in faint regions.

This report is a preliminary investigation of imaging capabilities including phase errors, realistic spectral structure, and using components of the ngVLA appropriate for the given spatial scales in source structure. The choice of Core antennas and TCLEAN parameters were not optimized, besides ensuring reasonable Fourier coverage down to 50 m spacings. Different choices may result in imaging improvements.

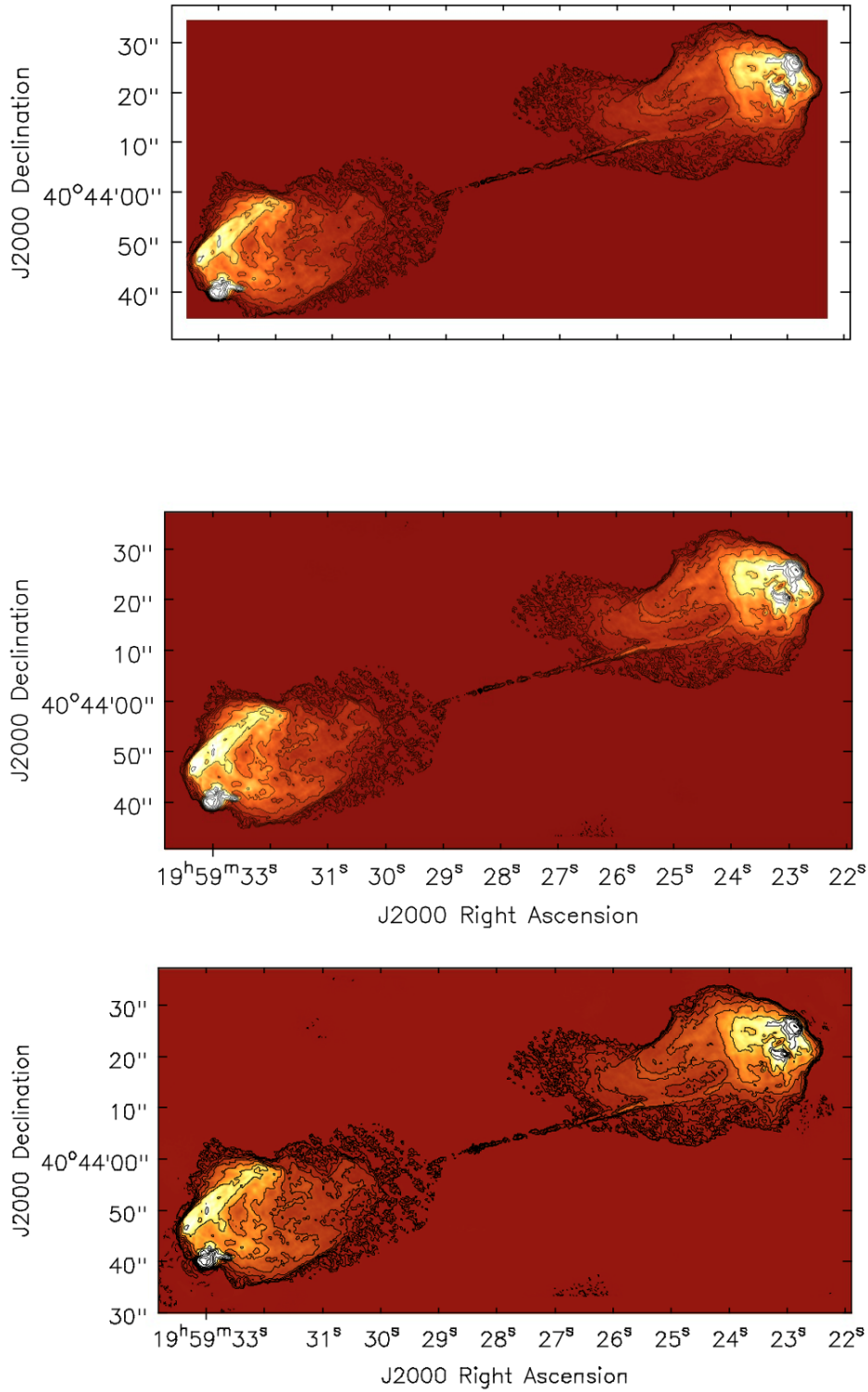


Figure 2: Top: Input model of Cygnus A at 8 GHz built from the VLA image. Middle: ngVLA image with Spiral and some Core antennas with just thermal noise. Bottom: ngVLA image with $\pm 1^\circ$ antenna-based phase errors constant in time and frequency. The contour levels are a geometric progression in factor two starting at $70 \mu\text{Jy beam}^{-1}$. The synthesized beam size is: $0.20'' \times 0.17''$, at 81° .

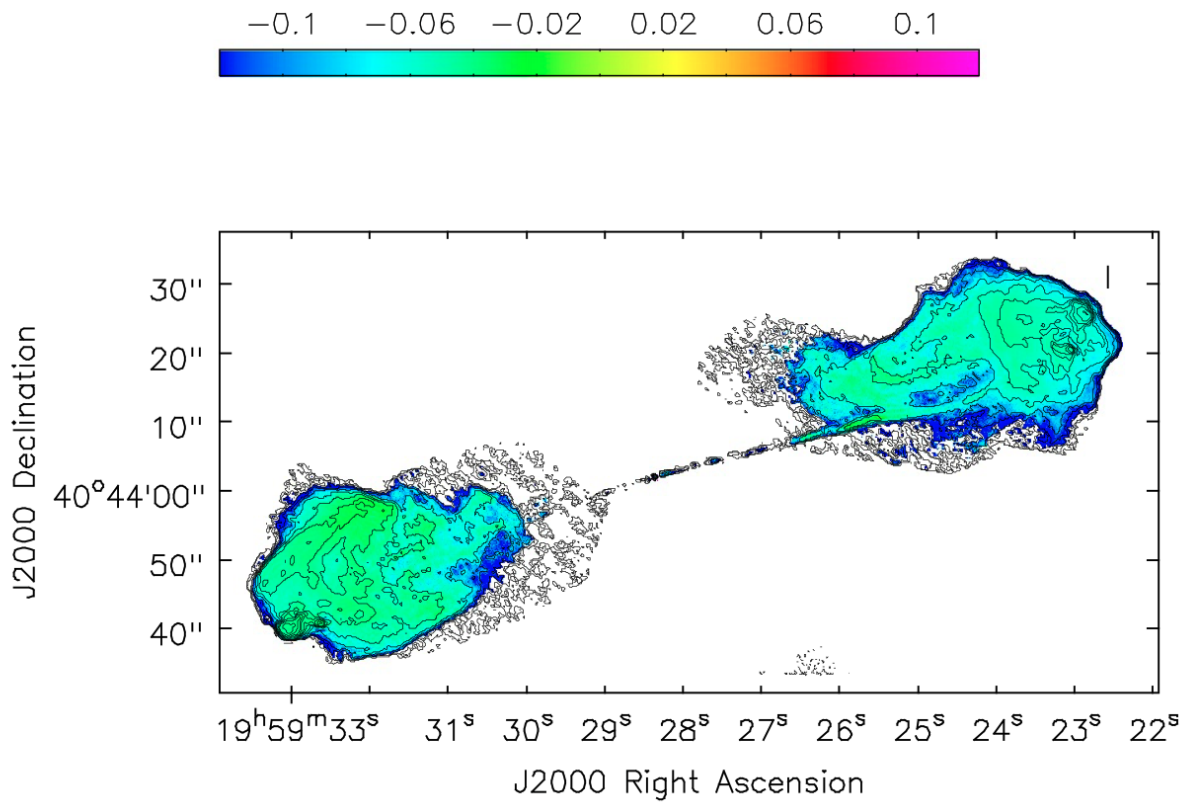


Figure 3: Fidelity image for the 8 GHz Cygnus A simulations with just thermal noise. Note that the results for the phase error images are similar in these higher S/N regions, and hence not shown. Contours are total intensity.

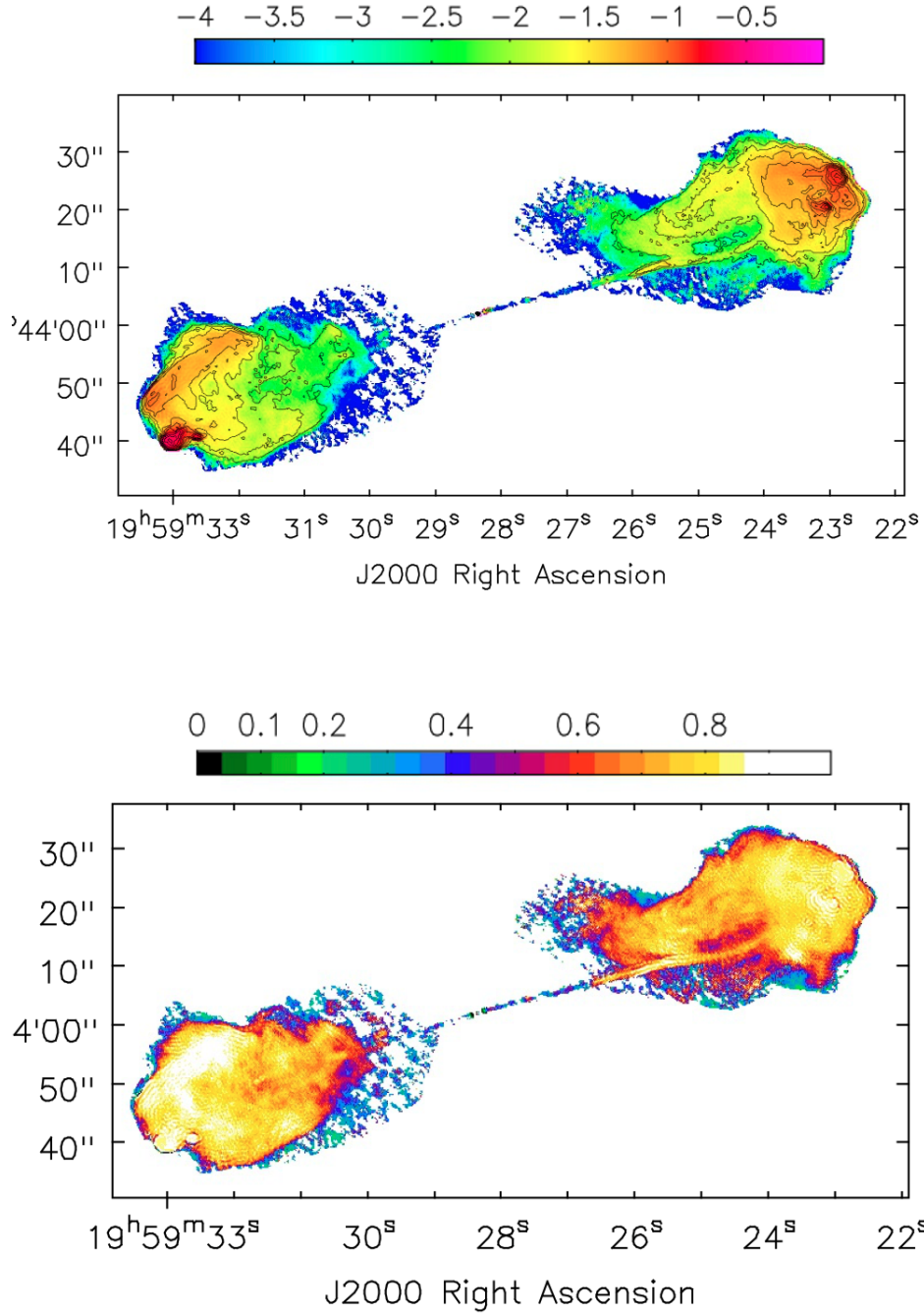


Figure 4: Top: Spectral index image with just thermal noise generated by TCLEAN with $n_{\text{terms}} = 2$. Bottom: Spectral index ratio image (model/data). The ratios are systematically less than one, implying have steeper spectra than the model (values < 1), in particular in the fainter regions of the source, where values can be 0.5, or less.